A HAMILTONIAN-PRESERVING SCHEME FOR THE LIOUVILLE EQUATION OF GEOMETRICAL OPTICS WITH PARTIAL TRANSMISSIONS AND REFLECTIONS[*]

SHI JIN[†] AND XIN WEN[‡]

Abstract. We construct a class of Hamiltonian-preserving numerical schemes for the Liouville equation of geometrical optics, with partial transmissions and reflections. This equation arises in the high frequency limit of the linear wave equation, with a discontinuous index of refraction. In our previous work [*Hamiltonian-preserving schemes for the Liouville equation of geometrical optics with discontinuous local wave speeds*, J. Comput. Phys. 214 (2006), pp. 672–697], we introduced the Hamiltonian-preserving schemes for the same equation when only complete transmissions or reflections occur at the interfaces. These schemes are extended in this paper to the general case of partial transmissions and reflections. The key idea is to build into the numerical flux the behavior of waves at the interface, namely, partial transmissions and reflections that satisfy Snell's law of refraction with the correct transmission and reflection coefficients. This scheme allows a hyperbolic stability condition, under which positivity, and stabilities in both l^1 and l^∞ norms, are established. Numerical experiments are carried out to study the numerical accuracy.

Key words. geometrical optics, Liouville equation, transmission and reflection, Hamiltonian-preserving schemes

AMS subject classifications. 35L45, 65M06, 70H99

DOI. 10.1137/050631343

1. Introduction. In this paper, we construct and study a numerical scheme for the Liouville equation in d-dimension:

$$(1.1) \qquad f_t + H_{\mathbf{v}} \cdot \nabla_{\mathbf{x}} f - H_{\mathbf{x}} \cdot \nabla_{\mathbf{v}} f = 0, \quad t > 0, \quad \mathbf{x}, \mathbf{v} \in R^d,$$

where the Hamiltonian H possesses the form

$$(1.2) \qquad H(\mathbf{x}, \mathbf{v}) = c(\mathbf{x})|\mathbf{v}| = c(\mathbf{x})\sqrt{v_1^2 + v_2^2 + \cdots + v_d^2}$$

with $c(\mathbf{x})$ being the local wave speed of the medium ($1/c(\mathbf{x})$ is the index of refraction); $f(t, \mathbf{x}, \mathbf{v})$ is the density distribution of particles depending on position $\mathbf{x}$, time t, and the slowness vector $\mathbf{v}$. We are concerned with the case when $c(\mathbf{x}) \in W^{1,\infty}$ with isolated *discontinuities* due to different media. The discontinuity in c corresponds to an *interface*, and as a consequence waves crossing this interface will undergo transmissions and reflections.

[†]Department of Mathematics, University of Wisconsin, Madison, WI 53706 and Department of Mathematical Sciences, Tsinghua University, Beijing 100084, P.R. China (jin@math.wisc.edu). This author's research was also supported in part by the Institute for Mathematics and its Applications (IMA) under a New Direction Visiting Professorship.

[‡]Institute of Computational Mathematics, Chinese Academy of Science, P. O. Box 2719, Beijing 100080, China (wenxin@amss.ac.cn).

The bicharacteristics of this Liouville equation (1.1) satisfy the Hamiltonian system

$$(1.3) \qquad \frac{d\mathbf{x}}{dt} = c(\mathbf{x})\frac{\mathbf{v}}{|\mathbf{v}|}, \quad \frac{d\mathbf{v}}{dt} = -c_{\mathbf{x}}|\mathbf{v}|.$$

In classical mechanics the Hamiltonian (1.2) of a particle remains a constant along the particle trajectory, even when it is being transmitted or reflected by the interface.

This Liouville equation arises in the phase space description of geometrical optics. It is the high frequency limit of the wave equation

$$(1.4) \qquad u_{tt} - c(\mathbf{x})^2\Delta u = 0, \quad t > 0, \quad \mathbf{x} \in R^d.$$

In the past, numerous numerical methods have been proposed for the wave equation (1.4) with discontinuous coefficients c; see [32] and references therein. However, our interest is in the high frequency waves, for which many current numerical methods such as the phase space based level set methods, are based on the Liouville equation (1.1) with smooth c; see [18, 25, 34]. Semiclassical limits of wave equations with transmissions and reflections at the interfaces were studied in [1, 33, 39]. A Liouville equation based level set method for the wave front, but with only reflection, was introduced in [9].

In our previous work [28] two classes of numerical schemes that are suitable for the Liouville equation (1.1) with a discontinuous local wave speed $c(\mathbf{x})$ were constructed. The designing principle there was to build the behavior of waves at the interface— either cross over with a changed velocity according to a constant Hamiltonian, or be reflected with a negative velocity (or momentum)—into the numerical flux; see also earlier works [36, 27]. These schemes were called *Hamiltonian-preserving schemes*. By providing an interface condition, it connects the two domains of Liouville equation with smooth coefficients. This gives a physically relevant selection criterion for a unique solution to the governing equation, which is linearly hyperbolic with singular (discontinuous or measure-valued) coefficients. For a plane wave hitting a flat interface, it selects the solution at the interface governed by *Snell's law of refraction* when the wave length is much shorter than the width of the interface while both lengths go to zero. Nevertheless, this is not the only physically relevant possibility to choose a solution across the interface. When the wave length is much longer than the width of the interface, while both lengths go to zero, the waves can be *partially* transmitted and reflected, and the transmission and reflection coefficients can be analytically computed [33].

The goal of this paper is to construct the numerical scheme which is suitable to deal with partial transmissions and reflections, with computable transmission and reflection coefficients. As in [28], we still use the *Hamiltonian-preserving* principle to determine the transmitted velocity across the interface. The new contribution of this paper is to incorporate the transmission and reflection coefficients into the numerical flux, in order to treat partial transmissions and reflections. This new, explicit scheme, like those in [27, 28], allows a typical hyperbolic stability condition $\Delta t = O(\Delta x, \Delta v)$, under which we also establish the positivity, and l^1 and l^∞ stability theory for the scheme.

In geometrical optics applications, one has to solve the Liouville equation like (1.1) with *measure-valued* initial data

$$(1.5) \qquad f(0, \mathbf{x}, \mathbf{v}) = \rho_0(\mathbf{x})\delta(\mathbf{v} - \mathbf{u}_0(\mathbf{x}));$$

see, for example, [38, 14, 25]. The solution at later time remains measure-valued (with finite or even infinite number of concentrations-corresponding to *multivalued* solutions in the physical space). Computation of multivalued solutions in geometrical optics and more generally in nonlinear PDEs has been a very active area of recent research; see [3, 4, 6, 5, 10, 17, 12, 13, 15, 19, 20, 21, 18, 26, 34, 37, 41].

Direct numerical methods (DNM) for the Liouville equation with measure-valued initial data (1.5), which approximate the initial delta function first, then evolve the Liouville equation, could suffer from a poor numerical resolution due to the numerical approximation of the initial data of delta function as well as numerical dissipation [24]. The level set method proposed in [24, 25] decomposes the density distribution f into the bounded level set functions obeying the same Liouville equation, which greatly enhances the numerical resolution. One only involves numerically the delta function at the output time when the moments—which has delta functions in their integrands—need to be evaluated numerically.

However, the extension of this density distribution decomposing approach to the case of partial transmission and reflection is not straightforward. In particular, as the number of transmissions and reflections increase in time, so does the number of needed level set functions satisfying (1.1). This difficulty was already pointed out in [9]. In this paper, when dealing with the measure-valued initial data (1.5) we will just use the DNM. This does not offer the same resolution as those in [28]. It remains an open question on how to extend the decomposition idea of [24, 25] to the case of partial transmissions and reflections.

This paper is organized as follows. In section 2, we present the behavior of waves at an interface, which guides the designing of our scheme. We also give an interface condition (2.5) which allows us to define the analytic solution to the Liouville equation (1.1) with singular coefficients. We present the scheme in 1d in section 3 and study its positivity and stability in both l^∞ and l^1 norms. We extend the scheme to the two space dimension in section 4 in the simple case of an interface aligning with the grids. Numerical examples are given in section 5 to verify the accuracy of the scheme. We make some concluding remarks in section 6.

2. The behavior of waves at an interface.

2.1. Transmissions and reflections at the interface.
In geometrical optics, when a wave moves with its density distribution governed by the Liouville equation (1.1), *its Hamiltonian $H = c|\mathbf{v}|$ should be preserved across the interface*

$$(2.1) \qquad c^+|\mathbf{v}^+| = c^-|\mathbf{v}^-|,$$

where the superscripts $\pm$ indicate the right and left limits of the quantity at the interface. The wave can be partly reflected and partly transmitted. The condition (2.1) can be used to determine the particle velocity on one side of the interface from its value on the other side. When a plane wave hits a flat interface, this condition is equivalent to Snell's law of refraction [28]:

$$(2.2) \qquad \frac{\sin\theta_i}{c^-} = \frac{\sin\theta_t}{c^+}$$

and the reflection law

$$(2.3) \qquad \theta_r = \theta_i,$$
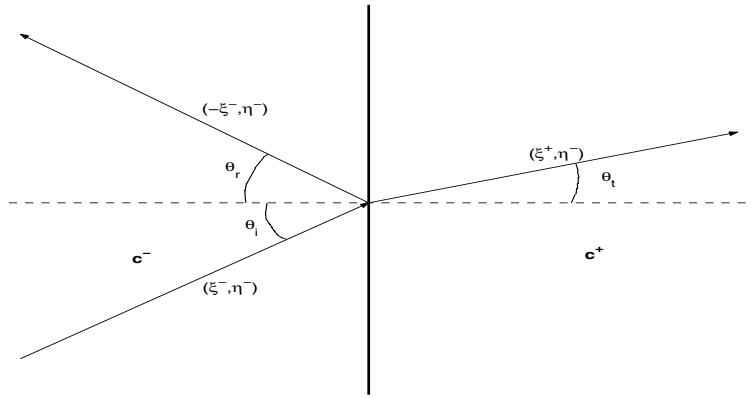
FIG. 2.1. *Wave transmission and reflection at an interface.*

where θ_i, θ_t, and θ_r stand for angles of incident and transmitted and reflected waves; see Figure 2.1. The reflection coefficient is given by

$$(2.4) \qquad \alpha^R = \left(\frac{c^+ \cos\theta_i - c^- \cos\theta_t}{c^+ \cos\theta_i + c^- \cos\theta_t} \right)^2$$

while the transmission coefficient is $\alpha^T = 1 - \alpha^R$; see, for example, [1, 33, 39].

We will discuss this behavior in more detail in 1D and 2D, respectively.

- The 1D case is simpler. Consider the case when, at an interface, the characteristic on the left of the interface is given by $\xi^- > 0$. Then with probability $\alpha^R = \left(\frac{c^+ - c^-}{c^+ + c^-} \right)^2$, the wave is reflected by the interface with a new velocity $-\xi^-$, and with probability $\alpha^T = 1 - \alpha^R$ it will cross the interface with the new velocity $\xi^+ = \frac{c^-}{c^+}\xi^-$ determined by (2.1).

- The 2D case, when an incident wave hits a vertical interface (see Figure 2.1). Let $\mathbf{x} = (x, y), \mathbf{v} = (\xi, \eta)$. Assume that the incident wave has a velocity (ξ^-, η^-) to the left side of the interface, with $\xi^- > 0$. Since the interface is vertical, (1.3) implies that η is not changed when the wave crosses the interface. There are two possibilities:

  1) $\left(\frac{c^-}{c^+} \right)^2 (\xi^-)^2 + \left[\left(\frac{c^-}{c^+} \right)^2 - 1 \right] (\eta^-)^2 > 0$. In this case the wave can partially transmit and partially be reflected. With probability $\alpha^R = \left(\frac{c^+\gamma^- - c^-\gamma^+}{c^+\gamma^- + c^-\gamma^+} \right)^2$ the wave is reflected with a new velocity $(-\xi^-, \eta^-)$, where

  $$\gamma^+ = \cos(\theta_t) = \frac{\xi^+}{\sqrt{(\xi^+)^2 + (\eta^-)^2}}, \quad \gamma^- = \cos(\theta_i) = \frac{\xi^-}{\sqrt{(\xi^-)^2 + (\eta^-)^2}}.$$

  With probability $\alpha^T = 1 - \alpha^R$ it will be transmitted with the new velocity (ξ^+, η^-), where

  $$\xi^+ = \sqrt{ \left(\frac{c^-}{c^+} \right)^2 (\xi^-)^2 + \left[\left(\frac{c^-}{c^+} \right)^2 - 1 \right] (\eta^-)^2 },$$

is obtained using (2.1).

2) $c^- < c^+$ and $\left(\frac{c^-}{c^+}\right)^2 (\xi^-)^2 + \left[\left(\frac{c^-}{c^+}\right)^2 - 1\right] (\eta^-)^2 < 0$. In this case, it is impossible for the wave to transmit, so the wave will be completely reflected with velocity $(-\xi^-, \eta^-)$.

If $\xi^- < 0$, similar behavior can also be analyzed using the constant Hamiltonian condition (2.1).

2.2. The interface condition for density distribution. The solution to the Liouville equation (1.1), which is linearly hyperbolic, can be solved by the method of characteristics. Namely, the density distribution f remains a constant along a bicharacteristic. However, with partial transmissions and reflections, this is no longer true, since f needs to be determined from two bicharacteristics, one accounting for the transmission and the other for reflection. Therefore, we use the following condition at the interface:

$$(2.5) \qquad f(t, \mathbf{x}^+, \mathbf{v}^+) = \alpha^T f(t, \mathbf{x}^-, \mathbf{v}^-) + \alpha^R f(t, \mathbf{x}^+, -\mathbf{v}^+),$$

where $\mathbf{v}^-$ is defined from $\mathbf{v}^+$ through the constant Hamiltonian condition (2.1), α^T and α^R are the transmission and reflection coefficients which add up to 1 and vary with $\mathbf{v}^+$ except in the 1D case. *This is the main idea of this paper*, and will be used in constructing the numerical flux across the interface in the next section. As will be seen in the next section, our scheme incorporates the interface condition into the numerical flux.

For hyperbolic systems with discontinuous coefficients, renormalized solution was introduced by DiPerna and Lions [11], and further extended in [7, 8, 22, 23] for uniqueness and stability. The renormalized solution idea cannot be applied here since the coefficients can be measure-valued. Our approach here is to use the interface condition (2.5) to connect two domains in which the Liouville equation has smooth Hamiltonians. Concretely, we define the solution for (1.1) when the local wave speed has discontinuities as follows.

DEFINITION 2.1. *The analytic solution for the Liouville equation (1.1) when the local wave speed c has discontinuities is constructed by method of characteristics away from the interface plus the interface condition (2.5).*

Below we justify the well-posedness of the initial value problem, for the simple case of a step function c with a vertical interface. The more general situation remains to be worked out and will be deferred to a future work.

Consider the simple case that the local wave speed $c(\mathbf{x}), \mathbf{x} \in R^d$ is piecewise constant as follows:

$$(2.6) \qquad c(\mathbf{x}) = \begin{cases} c^- & x_1 < 0 \\ c^+ & x_1 > 0, \end{cases}$$

where we assume $c^- < c^+$. We will also exclude some singular points, working in the domain defined by

$$(2.7) \qquad \Omega = \left\{ (\mathbf{x}, \mathbf{v}) | \mathbf{x} \in R^d, \mathbf{v} \in R^d \backslash \{\mathbf{0}\} \right\} \backslash \{(\mathbf{x}, \mathbf{v}) | x_1 = v_1 = 0\}.$$

We have the following theorem.

THEOREM 2.1. *Assume the initial data $f(0, \mathbf{x}, \mathbf{v})$ has a compact support in $\mathbf{v}$. With the solution defined in Definition 2.1, the initial value problem to*

$$(2.8) \qquad f_t + H_{\mathbf{v}} \cdot \nabla_{\mathbf{x}} f - H_{\mathbf{x}} \cdot \nabla_{\mathbf{v}} f = 0, \quad t > 0, \quad (\mathbf{x}, \mathbf{v}) \in \Omega,$$

with H given by (1.2), c given by (2.6), and Ω given by (2.7), is well-posed in l^∞ and l^1 norms.

Proof. The proof is based on explicit construction of the analytical solution $f(T, \mathbf{x}, \mathbf{v})$. The l^∞ stability follows from the maximum principle, while the key for the l^1 stability is to prove that *the Liouville theorem (volume preserving for a Hamiltonian flow) holds at the interface for partial tranmissions and reflections.*

To make the following description easier, we define a function extended from the local wave speed (2.6)

$$(2.9) \qquad \widetilde{c}(\mathbf{x}, \mathbf{v}) = \begin{cases} c^- & x_1 < 0 \\ c^+ & x_1 > 0 \\ c^- & x_1 = 0, \ v_1 < 0 \\ c^+ & x_1 = 0, \ v_1 > 0, \end{cases}$$

which is defined on the whole definition domain Ω. The values of $\widetilde{c}(\mathbf{x}, \mathbf{v})$ on $x_1 = 0$, however, are not crucial as long as they are positive.

Split the domain Ω into two parts $\Omega = \Omega_1 \cup \Omega_2$ with

$$\Omega_1 = \left\{ (\mathbf{x}, \mathbf{v}) \in \Omega \left| x_1 \left(x_1 - \widetilde{c}(\mathbf{x}, \mathbf{v}) \frac{v_1}{|\mathbf{v}|} T \right) > 0 \text{ or } \left(x_1 - \widetilde{c}(\mathbf{x}, \mathbf{v}) \frac{v_1}{|\mathbf{v}|} T \right) = 0 \right. \right\},$$

$$\Omega_2 = \left\{ (\mathbf{x}, \mathbf{v}) \in \Omega \left| x_1 \left(x_1 - \widetilde{c}(\mathbf{x}, \mathbf{v}) \frac{v_1}{|\mathbf{v}|} T \right) < 0 \text{ or } x_1 = 0 \right. \right\},$$

where Ω_1 consists of those points whose positions are not on the interface, and when tracing back along the bicharacteristics, will not hit the interface within time T, except possibly the end point. We further split domain Ω_1, Ω_2 as $\Omega_1 = \Omega_1^- \cup \Omega_1^+$, $\Omega_2 = \Omega_2^- \cup \Omega_2^+$ with

$$\Omega_1^- = \{ (\mathbf{x}, \mathbf{v}) \in \Omega_1 | x_1 < 0 \},$$
$$\Omega_1^+ = \{ (\mathbf{x}, \mathbf{v}) \in \Omega_1 | x_1 > 0 \},$$
$$\Omega_2^- = \left\{ (\mathbf{x}, \mathbf{v}) \in \Omega_2 \left| \left(x_1 - \widetilde{c}(\mathbf{x}, \mathbf{v}) \frac{v_1}{|\mathbf{v}|} T \right) > 0 \right. \right\},$$
$$\Omega_2^+ = \left\{ (\mathbf{x}, \mathbf{v}) \in \Omega_2 \left| \left(x_1 - \widetilde{c}(\mathbf{x}, \mathbf{v}) \frac{v_1}{|\mathbf{v}|} T \right) < 0 \right. \right\}.$$

For $(\mathbf{x}, \mathbf{v}) \in \Omega_1$, one has

$$(2.10) \qquad f(T, \mathbf{x}, \mathbf{v}) = f\left(0, \mathbf{x} - c^- \frac{\mathbf{v}}{|\mathbf{v}|} T, \mathbf{v} \right), \quad (\mathbf{x}, \mathbf{v}) \in \Omega_1^-,$$

$$(2.11) \qquad f(T, \mathbf{x}, \mathbf{v}) = f\left(0, \mathbf{x} - c^+ \frac{\mathbf{v}}{|\mathbf{v}|} T, \mathbf{v} \right), \quad (\mathbf{x}, \mathbf{v}) \in \Omega_1^+.$$

Define a subset of Ω_2^-

$$\Omega_{2,s} = \left\{ (\mathbf{x}, \mathbf{v}) \in \Omega_2^- \left| \left(\frac{c^-}{c^+} \right)^2 |\mathbf{v}|^2 \leq v_2^2 + \cdots + v_d^2 \right. \right\}.$$

For $(\mathbf{x}, \mathbf{v}) \in \Omega_2$, one has

$$(2.12) \quad f(T, \mathbf{x}, \mathbf{v}) = f(0, \mathbf{x_R}, \mathbf{v_R}), \qquad\qquad\qquad (\mathbf{x}, \mathbf{v}) \in \Omega_{2,s},$$
$$f(T, \mathbf{x}, \mathbf{v}) = \alpha_T(\mathbf{v_T}) f(0, \mathbf{x_T}, \mathbf{v_T}) + \alpha_R(\mathbf{v_R}) f(0, \mathbf{x_R}, \mathbf{v_R}), \quad (\mathbf{x}, \mathbf{v}) \in \Omega_2 \backslash \Omega_{2,s},$$
$$(2.13)$$

where $\alpha_T(\mathbf{v}), \alpha_R(\mathbf{v})$ denote the transmission and reflection coefficients determined by the incident wave slowness vector $\mathbf{v}$, with condition $\alpha_T(\mathbf{v}) + \alpha_R(\mathbf{v}) = 1$. In geometrical optics, the transmission coefficient also satisfies $\alpha_T(\mathbf{v_T}) = \alpha_T(\mathbf{v_R})$ for the slowness vectors $\mathbf{v_T}, \mathbf{v_R}$ appearing in (2.13), thus it holds that $\alpha_T(\mathbf{v_T}) + \alpha_R(\mathbf{v_R}) = 1$. This contributes to the maximum principle of the solution for (1.1). The positions and slowness vectors $\mathbf{x_T}, \mathbf{v_T}, \mathbf{x_R}, \mathbf{v_R}$ can be explicitly expressed by $\mathbf{x}, \mathbf{v}$ as follows

$$(2.14) \qquad v_{T,1}^2 = \left[\frac{\widehat{c}\,|\mathbf{v}|}{\widehat{c}_T} \right]^2 - v_2^2 - \cdots - v_d^2, \quad v_{T,1} v_1 > 0,$$

$$(2.15) \qquad v_{T,i} = v_i, \quad i = 2, \ldots, d,$$

$$(2.16) \qquad x_{T,1} = \frac{(\widehat{c}_T)^2 v_{T,1}}{|\mathbf{v}|\widehat{c}} \left(\frac{x_1 |\mathbf{v}|}{\widehat{c}\, v_1} - T \right),$$

$$(2.17) \qquad x_{T,i} = x_i - v_i \frac{x_1}{v_1} + \frac{(\widehat{c}_T)^2 v_i}{|\mathbf{v}|\widehat{c}} \left(\frac{x_1 |\mathbf{v}|}{\widehat{c}\, v_1} - T \right), \quad i = 2, \ldots, d,$$

$$(2.18) \qquad v_{R,1} = -v_1, \qquad v_{R,i} = v_i, \quad i = 2, \ldots, d,$$

$$(2.19) \qquad x_{R,1} = \frac{\widehat{c}\, v_1}{|\mathbf{v}|} \left(T - \frac{x_1 |\mathbf{v}|}{\widehat{c}\, v_1} \right),$$

$$(2.20) \qquad x_{R,i} = x_i - v_i \frac{x_1}{v_1} - \frac{\widehat{c}\, v_i}{|\mathbf{v}|} \left(T - \frac{x_1 |\mathbf{v}|}{\widehat{c}\, v_1} \right), \quad i = 2, \ldots, d,$$

where $\widehat{c}, \widehat{c}_T$ are given by

$$\begin{aligned} \widehat{c} = c^-, \quad \widehat{c}_T = c^+, \qquad & \text{for } (\mathbf{x}, \mathbf{v}) \in \Omega_2^-, \\ \widehat{c} = c^+, \quad \widehat{c}_T = c^-, \qquad & \text{for } (\mathbf{x}, \mathbf{v}) \in \Omega_2^+. \end{aligned}$$

Since the solution $f(T, \mathbf{x}, \mathbf{v})$ can be explicitly expressed as (2.10), (2.11), (2.12), and (2.13), we have proved the existence and uniqueness of the solution for the initial value problem in Theorem 2.1. The l^∞ stability follows easily from the maximum principle and linearity of the Liouville equation.

In the following we prove the l^1-stability of the solution for this initial value problem. Define the l^1-norm of the solution as

$$|f|_1 = \int_\Omega |f(t, \mathbf{x}, \mathbf{v})| d\mathbf{x} d\mathbf{v}.$$

Due to the linearity of the Liouville equation, one only needs to prove that when the initial value is bounded in l^1-norm, then the solution remains bounded in l^1-norm at later time. Assume $|f(0, \mathbf{x}, \mathbf{v})|_1$ exists, we now investigate the relation between $|f(T, \mathbf{x}, \mathbf{v})|_1$ and $|f(0, \mathbf{x}, \mathbf{v})|_1$.

Define the sets

$$\Omega_3^- = \left\{ (\mathbf{x}, \mathbf{v}) \in \Omega \,\middle|\, \exists (\mathbf{y}, \mathbf{v}) \in \Omega_1^- \text{ s.t. } \mathbf{x} = \mathbf{y} - c(\mathbf{y}) \frac{\mathbf{v}}{|\mathbf{v}|} T \right\},$$

$$\Omega_3^+ = \left\{ (\mathbf{x}, \mathbf{v}) \in \Omega \,\middle|\, \exists (\mathbf{y}, \mathbf{v}) \in \Omega_1^+ \text{ s.t. } \mathbf{x} = \mathbf{y} - c(\mathbf{y}) \frac{\mathbf{v}}{|\mathbf{v}|} T \right\},$$

$$\Omega_{4,s} = \left\{ (\mathbf{x}, \mathbf{v}) \in \Omega \,\middle|\, x_1 < 0, \; x_1 + c^- \frac{v_1}{|\mathbf{v}|} T \geq 0, \; \left(\frac{c^-}{c^+} \right)^2 |\mathbf{v}|^2 \leq v_2^2 + \cdots + v_d^2 \right\},$$

$$\Omega_4 = \Omega \backslash \{ \Omega_3^- \cup \Omega_3^+ \cup \Omega_{4,s} \}.$$

One has

$$|f(T, \mathbf{x}, \mathbf{v})|_1 = \int_{\Omega_1^-} |f(T, \mathbf{x}, \mathbf{v})| d\mathbf{x} d\mathbf{v} + \int_{\Omega_1^+} |f(T, \mathbf{x}, \mathbf{v})| d\mathbf{x} d\mathbf{v}$$

$$(2.21) \qquad + \int_{\Omega_{2,s}} |f(T, \mathbf{x}, \mathbf{v})| d\mathbf{x} d\mathbf{v} + \int_{\Omega_2 \backslash \Omega_{2,s}} |f(T, \mathbf{x}, \mathbf{v})| d\mathbf{x} d\mathbf{v}.$$

For the first part in (2.21), since the map $(\mathbf{x}, \mathbf{v}) \to (\mathbf{x} + c^- \frac{\mathbf{v}}{|\mathbf{v}|} T, \mathbf{v})$ is volume-preserving, (2.10) gives

$$(2.22) \qquad \int_{\Omega_1^-} |f(T, \mathbf{x}, \mathbf{v})| d\mathbf{x} d\mathbf{v} = \int_{\Omega_1^-} \left| f\left(0, \mathbf{x} - c^- \frac{\mathbf{v}}{|\mathbf{v}|} T, \mathbf{v}\right) \right| d\mathbf{x} d\mathbf{v}$$

$$= \int_{\Omega_3^-} |f(0, \mathbf{x}, \mathbf{v})| d\mathbf{x} d\mathbf{v}.$$

In the same way, the second part in (2.21) holds

$$(2.23) \qquad \int_{\Omega_1^+} |f(T, \mathbf{x}, \mathbf{v})| d\mathbf{x} d\mathbf{v} = \int_{\Omega_3^+} |f(0, \mathbf{x}, \mathbf{v})| d\mathbf{x} d\mathbf{v}.$$

To calculate the last two parts in (2.21), we need to investigate the Jacobians of the maps $(\mathbf{x_T}, \mathbf{v_T}) \to (\mathbf{x}, \mathbf{v})$ and $(\mathbf{x_R}, \mathbf{v_R}) \to (\mathbf{x}, \mathbf{v})$. From (2.14)–(2.20), these two maps can be explicitly written out. The nonzero elements in the two Jacobian matrices include

$$\frac{\partial x_1}{\partial x_{T,1}}, \frac{\partial x_1}{\partial v_{T,1}}, \frac{\partial x_1}{\partial v_{T,2}}, \dots, \frac{\partial x_1}{\partial v_{T,d}},$$

$$\frac{\partial x_i}{\partial x_{T,1}}, \frac{\partial x_i}{\partial x_{T,i}}, \frac{\partial x_i}{\partial v_{T,1}}, \frac{\partial x_i}{\partial v_{T,2}}, \dots, \frac{\partial x_i}{\partial v_{T,d}}, \quad i = 2, \dots, d,$$

$$\frac{\partial v_1}{\partial v_{T,i}}, \quad i = 1, 2, \dots, d, \qquad \frac{\partial v_i}{\partial v_{T,i}}, \quad i = 2, \dots, d,$$

$$\frac{\partial x_1}{\partial x_{R,1}}, \frac{\partial x_1}{\partial v_{R,1}}, \frac{\partial x_1}{\partial v_{R,2}}, \dots, \frac{\partial x_1}{\partial v_{R,d}},$$

$$\frac{\partial x_i}{\partial x_{R,1}}, \frac{\partial x_i}{\partial x_{R,i}}, \frac{\partial x_i}{\partial v_{R,1}}, \frac{\partial x_i}{\partial v_{R,2}}, \dots, \frac{\partial x_i}{\partial v_{R,d}}, \quad i = 2, \dots, d,$$

$$\frac{\partial v_i}{\partial v_{R,i}}, \quad i = 1, 2, \dots, d,$$

from which only the diagonal elements influence the Jacobians. They are

$$\frac{\partial x_1}{\partial x_{T,1}} = \left(\frac{\widehat{c}}{\widehat{c}_T} \right)^2 \frac{v_1}{v_{T,1}},$$

$$\frac{\partial x_i}{\partial x_{T,i}} = 1, \quad i = 2, \dots, d,$$

$$\frac{\partial v_1}{\partial v_{T,1}} = \left(\frac{\widehat{c}_T}{\widehat{c}} \right)^2 \frac{v_{T,1}}{v_1},$$

$$\frac{\partial v_i}{\partial v_{T,i}} = 1, \quad i = 2, \dots, d,$$

$$\frac{\partial x_1}{\partial x_{R,1}} = -1, \qquad \frac{\partial x_i}{\partial x_{R,i}} = 1, \quad i = 2, \ldots, d,$$

$$\frac{\partial v_1}{\partial v_{R,1}} = -1, \qquad \frac{\partial v_i}{\partial v_{R,i}} = 1, \quad i = 2, \ldots, d.$$

Thus it is verified that the two maps $(\mathbf{x_T}, \mathbf{v_T}) \to (\mathbf{x}, \mathbf{v})$ and $(\mathbf{x_R}, \mathbf{v_R}) \to (\mathbf{x}, \mathbf{v})$ are *volume-preserving*.

For the third part in (2.21), from (2.12) one has

$$(2.24) \quad \int_{\Omega_{2,s}} |f(T, \mathbf{x}, \mathbf{v})| d\mathbf{x} d\mathbf{v} = \int_{\Omega_{2,s}} |f(0, \mathbf{x_R}, \mathbf{v_R})| d\mathbf{x} d\mathbf{v} = \int_{\Omega_{4,s}} |f(0, \mathbf{x}, \mathbf{v})| d\mathbf{x} d\mathbf{v}.$$

For the fourth part in (2.21), from (2.13) one has

$$\int_{\Omega_2 \setminus \Omega_{2,s}} |f(T, \mathbf{x}, \mathbf{v})| d\mathbf{x} d\mathbf{v} = \int_{\Omega_2 \setminus \Omega_{2,s}} \alpha_T(\mathbf{v_T}) |f(0, \mathbf{x_T}, \mathbf{v_T})| d\mathbf{x} d\mathbf{v}$$

$$+ \int_{\Omega_2 \setminus \Omega_{2,s}} \alpha_R(\mathbf{v_R}) |f(0, \mathbf{x_R}, \mathbf{v_R})| d\mathbf{x} d\mathbf{v}$$

$$= \int_{\Omega_4} \alpha_T(\mathbf{v}) |f(0, \mathbf{x}, \mathbf{v})| d\mathbf{x} d\mathbf{v} + \int_{\Omega_4} \alpha_R(\mathbf{v}) |f(0, \mathbf{x}, \mathbf{v})| d\mathbf{x} d\mathbf{v}$$

$$(2.25) \qquad\qquad = \int_{\Omega_4} |f(0, \mathbf{x}, \mathbf{v})| d\mathbf{x} d\mathbf{v}.$$

Together with (2.21), (2.22), (2.23), (2.24), and (2.25), one gets

$$|f(T, \mathbf{x}, \mathbf{v})|_1 = \int_{\Omega_3^-} |f(0, \mathbf{x}, \mathbf{v})| d\mathbf{x} d\mathbf{v} + \int_{\Omega_3^+} |f(0, \mathbf{x}, \mathbf{v})| d\mathbf{x} d\mathbf{v}$$

$$+ \int_{\Omega_{4,s}} |f(0, \mathbf{x}, \mathbf{v})| d\mathbf{x} d\mathbf{v} + \int_{\Omega_4} |f(0, \mathbf{x}, \mathbf{v})| d\mathbf{x} d\mathbf{v}$$

$$= |f(0, \mathbf{x}, \mathbf{v})|_1.$$

This is the l^1-stability—in fact l^1 preservation—of the solution for the initial value problem in Theorem 2.1. □

Remark 2.1. In [2], a classical-classical coupling model that connects two domains of classical mechanics with constant potentials with a classical domain $[a, b]$ in between where the potential is variable was introduced, where the interface conditions at a and b were given. When $a = b$, their interface conditions reduce to (2.5).

3. The scheme in 1D.

3.1. The numerical flux. We now describe our finite difference scheme for the 1D Liouville equation

$$(3.1) \qquad\qquad f_t + c(x)\mathrm{sign}(\xi)f_x - c_x|\xi|f_\xi = 0.$$

We employ a uniform mesh with grid points at $x_{i+\frac{1}{2}}, i = 0, \ldots, N$, in the x-direction and $\xi_{j+\frac{1}{2}}, j = 0, \ldots, M$ in the ξ-direction. The cells are centered at (x_i, ξ_j), $i = 1, \ldots, N, j = 1, \ldots, M$ with $x_i = \frac{1}{2}(x_{i+\frac{1}{2}} + x_{i-\frac{1}{2}})$ and $\xi_j = \frac{1}{2}(\xi_{j+\frac{1}{2}} + \xi_{j-\frac{1}{2}})$. The uniform mesh size is denoted by $\Delta x = x_{i+\frac{1}{2}} - x_{i-\frac{1}{2}}, \Delta \xi = \xi_{j+\frac{1}{2}} - \xi_{j-\frac{1}{2}}$. We also assume a uniform time step Δt and the discrete time is given by $0 = t_0 < t_1 < \cdots < t_L = T$.

We introduce the mesh ratios $\lambda_x^t = \frac{\Delta t}{\Delta x}, \lambda_\xi^t = \frac{\Delta t}{\Delta \xi}$, assumed to be fixed. The cell average of f is defined by

$$f_{ij} = \frac{1}{\Delta x \Delta \xi} \int_{x_{i-\frac{1}{2}}}^{x_{i+\frac{1}{2}}} \int_{\xi_{j-\frac{1}{2}}}^{\xi_{j+\frac{1}{2}}} f(x,\xi,t) d\xi dx.$$

We assume the local wave speed is Lipschitz continuous except at its isolated discontinuous points. Assume that the discontinuous points of the wave speed c are located at the grid points. Let the left and right limits of $c(x)$ at point $x_{i+1/2}$ be $c_{i+\frac{1}{2}}^+$ and $c_{i+\frac{1}{2}}^-$, respectively. Note that if c is continuous at $x_{j+1/2}$, then $c_{i+\frac{1}{2}}^+ = c_{i+\frac{1}{2}}^-$. We approximate c by a piecewise linear function

$$c(x) \approx c_{j-1/2}^+ + \frac{c_{j+1/2}^- - c_{j-1/2}^+}{\Delta x}(x - x_{j-1/2}).$$

We also define the average wave speed as $c_i = \frac{1}{2}(c_{i-\frac{1}{2}}^+ + c_{i+\frac{1}{2}}^-)$. We will adopt the flux splitting technique used in [36, 27, 28]. The semidiscrete scheme (with time continuous) reads

$$(3.2) \quad (f_{ij})_t + \frac{c_i \text{sign}(\xi_j)}{\Delta x}(f_{i+\frac{1}{2},j}^- - f_{i-\frac{1}{2},j}^+) - \frac{c_{i+\frac{1}{2}}^- - c_{i-\frac{1}{2}}^+}{\Delta x \Delta \xi}|\xi_j|(f_{i,j+\frac{1}{2}} - f_{i,j-\frac{1}{2}}) = 0,$$

where the numerical fluxes $f_{i,j+\frac{1}{2}}$ are defined using the upwind discretization. Since the characteristics of the Liouville equation may be different on the two sides of the interface, the corresponding numerical fluxes should also be different. The essential part of our algorithm is to define the split numerical fluxes $f_{i+\frac{1}{2},j}^-, f_{i-\frac{1}{2},j}^+$ at each cell interface. We will use (2.5) to define these fluxes.

Assume c is discontinuous at $x_{i+\frac{1}{2}}$. Consider the case $\xi_j > 0$. Using upwind scheme, $f_{i+\frac{1}{2},j}^- = f_{ij}$. However, by (2.5),

$$f_{i+\frac{1}{2},j}^+ = \alpha^T f(t, x_{i+\frac{1}{2}}^-, \xi^-) + \alpha^R f(t, x_{i+\frac{1}{2}}^+, -\xi^+)$$

while ξ^- is obtained from $\xi^+ = \xi_j$ from (2.1). Since ξ^- may not be a grid point, we have to define it approximately. One can first locate the two cell centers that bound this velocity, and then use a linear interpolation to evaluate the needed numerical flux at ξ^-. The case of $\xi_j < 0$ is treated similarly. The detailed algorithm to generate the numerical flux is given below.

Algorithm I
- if $\xi_j > 0$
$$f_{i+\frac{1}{2},j}^- = f_{ij},$$
$$\xi' = \frac{c_{i+\frac{1}{2}}^+}{c_{i+\frac{1}{2}}^-}\xi_j$$
  - if $\xi_k \leq \xi' < \xi_{k+1}$ for some k
$$\alpha^R = \left(\frac{c_{i+\frac{1}{2}}^+ - c_{i+\frac{1}{2}}^-}{c_{i+\frac{1}{2}}^+ + c_{i+\frac{1}{2}}^-}\right)^2, \quad \alpha^T = 1 - \alpha^R$$
$$f_{i+\frac{1}{2},j}^+ = \alpha^T \left(\frac{\xi_{k+1} - \xi'}{\Delta \xi} f_{i,k} + \frac{\xi' - \xi_k}{\Delta \xi} f_{i,k+1}\right) + \alpha^R f_{i+1,k'}$$

$$\text{where } \xi_{k'} = -\xi_k$$

- end
- if $\xi_j < 0$
$$f^+_{i+\frac{1}{2},j} = f_{i+1,j},$$

$$\xi' = \frac{c^-_{i+\frac{1}{2}}}{c^+_{i+\frac{1}{2}}}\xi_j$$

  - if $\xi_k \leq \xi' < \xi_{k+1}$ for some k
$$\alpha^R = \left(\frac{c^+_{i+\frac{1}{2}} - c^-_{i+\frac{1}{2}}}{c^+_{i+\frac{1}{2}} + c^-_{i+\frac{1}{2}}}\right)^2, \quad \alpha^T = 1 - \alpha^R$$

$$f^-_{i+\frac{1}{2},j} = \alpha^T\left(\frac{\xi_{k+1} - \xi'}{\Delta\xi}f_{i+1,k} + \frac{\xi' - \xi_k}{\Delta\xi}f_{i+1,k+1}\right) + \alpha^R f_{i,k'}$$

$$\text{where } \xi_{k'} = -\xi_k$$

  - end

The above algorithm for evaluating numerical fluxes is of first order. One can obtain a second order flux by incorporating the slope limiter, such as the van Leer or minmod slope limiter [31], into the above algorithm. This can be achieved by replacing f_{ik} with $f_{ik} + \frac{\Delta x}{2}s_{ik}$, and replacing $f_{i+1,k}$ with $f_{i+1,k} - \frac{\Delta x}{2}s_{i+1,k}$ in the above algorithm for all possible index k, where s_{ik} is the slope limiter in the x-direction.

After the spatial discretization is specified, one can use any time discretization for the time derivative.

3.2. Positivity and l^∞ contraction. Since the exact solution of the Liouville equation is positive when the initial profile is, it is important that the numerical solution inherits this property.

We only consider the scheme using the first order numerical flux, and the forward Euler method in time. Without loss of generality, we consider the case $\xi_j > 0$ and $c^-_{i+\frac{1}{2}} < c^+_{i-\frac{1}{2}}$ for all i (the other cases can be treated similarly with the same conclusion). The scheme reads

$$\frac{f^{n+1}_{ij} - f^n_{ij}}{\Delta t} + c_i\frac{f_{ij} - (d_1 f_{i-1,k} + d_2 f_{i-1,k+1} + \alpha^R f_{i,k'})}{\Delta x} - \frac{c^-_{i+\frac{1}{2}} - c^+_{i-\frac{1}{2}}}{\Delta x}\xi_j\frac{f_{ij} - f_{i,j-1}}{\Delta\xi} = 0,$$

where d_1, d_2, α^R are nonnegative and $d_1 + d_2 = \alpha^T = 1 - \alpha^R$. We omit the superscript n of f. The above scheme can be rewritten as

$$f^{n+1}_{ij} = \left(1 - c_i\lambda^t_x - \frac{\left|c^-_{i+\frac{1}{2}} - c^+_{i-\frac{1}{2}}\right|}{\Delta x}|\xi_j|\lambda^t_\xi\right)f_{ij} + c_i\lambda^t_x\left(d_1 f_{i-1,k} + d_2 f_{i-1,k+1} + \alpha^R f_{i,k'}\right)$$

$$(3.3) \quad + \frac{\left|c^-_{i+\frac{1}{2}} - c^+_{i-\frac{1}{2}}\right|}{\Delta x}|\xi_j|\lambda^t_\xi f_{i,j-1}.$$

Now we investigate the positivity of scheme (3.3). This is to prove that if $f^n_{ij} \geq 0$ for all (i,j), then this is also true for f^{n+1}. Clearly one just needs to show that all of the coefficients before f^n are nonnegative. A sufficient condition for this is clearly

$$1 - c_i\lambda^t_x - \frac{\left|c^-_{i+\frac{1}{2}} - c^+_{i-\frac{1}{2}}\right|}{\Delta x}|\xi_j|\lambda^t_\xi \geq 0,$$

or

$$(3.4) \qquad \Delta t \max_{i,j} \left[\frac{c_i}{\Delta x} + \frac{\frac{\left| c^-_{i+\frac{1}{2}} - c^+_{i-\frac{1}{2}} \right|}{\Delta x} |\xi_j|}{\Delta \xi} \right] \leq 1.$$

The quantity $\frac{\left| c^-_{i+\frac{1}{2}} - c^+_{i-\frac{1}{2}} \right|}{\Delta x}$ now represents the wave speed gradient at its *smooth* point, which has a *finite* upper bound since $c \in W^{1,\infty}$. In addition, typically f has a compact support, so in practical computation ξ is confined in a bounded set. Thus our scheme allows a time step $\Delta t = O(\Delta x, \Delta \xi)$.

According to the study in [35], our second order scheme, which incorporates a slope limiter into the first order scheme, is positive under the half CFL condition, namely, the constant on the right-hand side of (3.4) is 1/2.

The above conclusion is drawn on the forward Euler time discretization. One can draw the same conclusion for the second order TVD Runge–Kutta time discretization [40].

The l^∞-contracting property of this scheme:

$$\|f^n\|_\infty \leq \|f^0\|_\infty$$

follows easily, because the coefficients in (3.3) are positive and the sum of them is 1.

3.3. The l^1-stability of the scheme. In this section we prove the l^1-stability of the scheme (with the first order numerical flux and the forward Euler method in time). For simplicity, we consider the case when the wave speed has only one discontinuity at grid point $x_{m+\frac{1}{2}}$ with $c^-_{m+\frac{1}{2}} > c^+_{m+\frac{1}{2}}$, and $c'(x) > 0$ at smooth points. The other cases, namely, when $c'(x) \leq 0$, or the wave speed having several discontinuity points with increased or decreased jumps, can be discussed similarly. Denote $\lambda_c \equiv c^+_{m+\frac{1}{2}} / c^-_{m+\frac{1}{2}} < 1$.

We consider the general case that $\xi_1 < 0, \xi_M > 0$. For this case, as adopted in [25, 28], the computational domain should exclude a set $O_\xi = \left\{ (x, \xi) \in \mathbb{R}^2 \,|\, \xi = 0 \right\}$, which causes singularity in the velocity field. For example, we can exclude the following index set:

$$D_o = \left\{ (i, j) \,\middle|\, |\xi_j| < \frac{\Delta \xi}{2} \right\},$$

from the computational domain.

Since $c(x)$ has a discontinuity, we also define an index set

$$D_l^4 = \{ (i, j) | x_i \leq x_m, \xi_j < \lambda_c \xi_1 \}.$$

As mentioned in [28], D_l^4 represents the area where waves come from outside of the domain $[x_1, x_N] \times [\xi_1, \xi_M]$. In order to implement our scheme conveniently, this index set is also excluded from the computational domain. Thus the computational domain is chosen as

$$(3.5) \qquad E_d = \{ (i, j) | i = 1, \ldots, N, j = 1, \ldots, M \} \setminus \left\{ D_o \cup D_l^4 \right\}.$$

As a result of excluding the index set D_o from the computational domain, the computational domain is split into two nonoverlapping parts:

$$E_d = \{ (i, j) \in E_d | \xi_j > 0 \} \cup \{ (i, j) \in E_d | \xi_j < 0 \} \equiv E_d^+ \cup E_d^-.$$

In [28] we analyzed the l^1-stability of the scheme on E_d^+ and E_d^- separately. Here we will conduct the analysis on the full phase space E_d since transmission and reflection waves coexist at the interface.

We define the l^1-norm of a numerical solution u_{ij} in the set E_d to be

$$(3.6) \qquad |f|_1 = \frac{1}{N_d} \sum_{(i,j) \in E_d} |f_{ij}|$$

with N_d being the number of elements in E_d.

Given the initial data $f_{ij}^0, (i,j) \in E_d$. Denote the numerical solution at time T to be $f_{ij}^L, (i,j) \in E_d$. To prove the l^1-stability, we need to show that $|f^L|_1 \le C|f^0|_1$.

Due to the linearity of the scheme, the equation for the error between the analytical and the numerical solutions is the same as (3.3), so in this section, f_{ij} will denote the error. We assume there is no error at the boundary, thus $f_{ij}^n = 0$ at the boundary. If the l^1-norm of the error introduced at each time step in the incoming boundary cells is ensured to be $o(1)$ part of $|f^n|_1$, our following analysis still applies.

Now denote

$$(3.7) \qquad A_i = \frac{1}{\Delta x} \left| c_{i+\frac{1}{2}}^- - c_{i-\frac{1}{2}}^+ \right|.$$

Since $c(x)$ is Lipschitz continuous at its smooth part, there exists an $A_u > 0$, such that $A_i < A_u, \forall i$. Assume also that there is an $C_m > 0$ such that $c_i > C_m, \forall i$. The finite difference scheme is given as follows:

- When $\xi_j > 0$
  1) if $i \ne m+1$,

  $$(3.8) \quad f_{ij}^{n+1} = \left(1 - A_i|\xi_j|\lambda_\xi^t - c_i\lambda_x^t\right) f_{ij} + A_i|\xi_j|\lambda_\xi^t f_{i,j+1} + c_i\lambda_x^t f_{i-1,j},$$

  2)

  $$f_{m+1,j}^{n+1} = \left(1 - A_{m+1}|\xi_j|\lambda_\xi^t - c_{m+1}\lambda_x^t\right) f_{m+1,j} + A_{m+1}|\xi_j|\lambda_\xi^t f_{m+1,j+1}$$
  $$(3.9) \qquad + c_{m+1}\lambda_x^t(d_{j1}f_{m,k} + d_{j2}f_{m,k+1} + \alpha^R f_{m+1,k'}).$$

- When $\xi_j < 0$
  3) if $i \ne m$,

  $$(3.10) \quad f_{ij}^{n+1} = \left(1 - A_i|\xi_j|\lambda_\xi^t - c_i\lambda_x^t\right) f_{ij} + A_i|\xi_j|\lambda_\xi^t f_{i,j+1} + c_i\lambda_x^t f_{i+1,j},$$

  4)

  $$f_{mj}^{n+1} = \left(1 - A_m|\xi_j|\lambda_\xi^t - c_m\lambda_x^t\right) f_{mj} + A_m|\xi_j|\lambda_\xi^t f_{m,j+1}$$
  $$(3.11) \qquad + c_m\lambda_x^t(d_{j1}f_{m+1,k} + d_{j2}f_{m+1,k+1} + \alpha^R f_{m,k'}),$$

where $0 \le d_{j1}, d_{j2} \le 1$ and $d_{j1} + d_{j2} = \alpha^T = 1 - \alpha^R = 1$. In (3.9) k is determined by $\xi_k \le \lambda_c \xi_j < \xi_{k+1}$ and $\xi_{k'} = -\xi_k$. In (3.11) k is determined by $\xi_k \le \frac{\xi_j}{\lambda_c} < \xi_{k+1}$ and $\xi_{k'} = -\xi_k$.

When summing up all absolute values of f_{ij}^{n+1} in (3.8)–(3.11), one typically gets the following inequality:

$$(3.12) \qquad |f^{n+1}|_1 \le \frac{1}{N_d} \sum_{(i,j) \in E_d} \alpha_{ij}|f_{ij}^n|,$$

where the coefficients α_{ij} are positive. One can check that, under the CFL condition (3.4), $\alpha_{ij} \leq 1 + 2A_u\Delta t$ except for possibly $(i,j) \in D^-_{m+1} \bigcup D^+_m$, where

$$D^-_{m+1} = \{(i,j) \in E^-_d | i = m+1\}, \quad D^+_m = \{(i,j) \in E^+_d | i = m\}.$$

We next derive the bounds for M^-, M^+ defined as

$$M^- = \max_{(m+1,j) \in D^-_{m+1}} \alpha_{m+1,j}, \quad M^+ = \max_{(m,j) \in D^+_m} \alpha_{m,j}.$$

Define the set

$$S^{m+1}_j = \left\{ j' \Big| \xi_{j'} < 0, \left| \frac{\xi_{j'}}{\lambda_c} - \xi_j \right| < \Delta\xi \right\} \quad \text{for} \ (m+1,j) \in D^-_{m+1}.$$

Let the number of elements in S^{m+1}_j be N^{m+1}_j. One can check that $N^{m+1}_j \leq 2\lambda_c + 1$ because every two elements $j'_1, j'_2 \in S^{m+1}_j$ satisfy $\left| \frac{\xi_{j'_1}}{\lambda_c} - \frac{\xi_{j'_2}}{\lambda_c} \right| \geq \frac{\Delta\xi}{\lambda_c}$.

On the other hand, one can easily check from (3.9) and (3.11), for $(m+1,j) \in D^-_{m+1}$, that

$$\alpha_{m+1,j} < 1 - c_{m+1}\lambda^t_x + c_m\lambda^t_x (2\lambda_c + 1)\alpha^T + \alpha^R c_{m+1}\lambda^t_x = 1 + \alpha^T(c_m + c_{m+1})\lambda^t_x + O(\Delta x),$$

so for sufficiently small Δx, M^- can be bounded by

$$M^- < 1 + 2\alpha^T(c_m + c_{m+1})\lambda^t_x.$$

Similarly, one can prove for sufficiently small Δx, M^+ is also bounded by

$$M^+ < 1 + 2\alpha^T(c_m + c_{m+1})\lambda^t_x.$$

Denote $M' = 2\alpha^T(c_m + c_{m+1})\lambda^t_x$. From (3.12),

$$|f^{n+1}|_1 < (1 + 2A_u\Delta t)|f^n|_1 + \frac{M'}{N_d} \sum_{(m+1,j) \in D^-_{m+1}} |f^n_{m+1,j}| + \frac{M'}{N_d} \sum_{(m,j) \in D^+_m} |f^n_{m,j}|.$$

(3.13)

Consecutively using (3.13) gives

$$|f^L|_1 < (1 + 2A_u\Delta t)^L \Bigg\{ |f^0|_1 + \frac{M'}{N_d} \sum_{n=0}^{L-1} \Bigg[\sum_{(m+1,j) \in D^-_{m+1}} |f^n_{m+1,j}| \Bigg]$$

(3.14)
$$+ \frac{M'}{N_d} \sum_{n=0}^{L-1} \Bigg[\sum_{(m,j) \in D^+_m} |f^n_{m,j}| \Bigg] \Bigg\}.$$

Define

(3.15) $$S_1 = \sum_{n=0}^{L-1} \Bigg[\sum_{(m+1,j) \in D^-_{m+1}} |f^n_{m+1,j}| \Bigg], \quad S_2 = \sum_{n=0}^{L-1} \Bigg[\sum_{(m,j) \in D^+_m} |f^n_{m,j}| \Bigg].$$

These two terms can be proved in the same way as in [29] to get

(3.16) $$S_1, S_2 < C_T N_d |f^0|_1,$$

where

(3.17) $$C_T \equiv \exp\left(\frac{2A_u}{C_m}(x_N - x_1)\right)\frac{1}{C_m \lambda_x^t}.$$

Combing (3.14) and (3.16),

$$\begin{aligned} |f^L|_1 &< (1 + 2A_u\Delta t)^L \left\{|f^0|_1 + 2C_T M'|f^0|_1\right\} \\ &= \exp\left(2A_u T\right)\left[1 + 2C_T M'\right]|f^0|_1 \\ &\equiv C|f^0|_1, \end{aligned}$$

where $C \equiv \exp\left(2A_u T\right)\left[1 + 2C_T M'\right]$.

Thus we prove the following theorem.

THEOREM 3.1. *Let $c(x) \in W^{1,\infty}$ have a discontinuity at one point, and be bounded below from zero, $c(x) > C_m > 0$. Assume f^0 has a finite l^1-norm defined (3.6) with a compact support in ξ. Then under the hyperbolic CFL condition (3.4), the solution yielded by the scheme (3.8)–(3.11) is stable in l^1-norm:*

$$|f^L|_1 < C|f^0|_1.$$

4. The scheme in two space dimension. Consider the 2D Liouville equation

(4.1) $$f_t + \frac{c(x,y)\xi}{\sqrt{\xi^2 + \eta^2}}f_x + \frac{c(x,y)\eta}{\sqrt{\xi^2 + \eta^2}}f_y - c_x\sqrt{\xi^2 + \eta^2}f_\xi - c_y\sqrt{\xi^2 + \eta^2}f_\eta = 0.$$

We employ a uniform mesh with grid points at $x_{i+\frac{1}{2}}, y_{j+\frac{1}{2}}, \xi_{k+\frac{1}{2}}, \eta_{l+\frac{1}{2}}$ in each direction. The cells are centered at $(x_i, y_j, \xi_k, \eta_l)$ with $x_i = \frac{1}{2}(x_{i+\frac{1}{2}} + x_{i-\frac{1}{2}}), y_j = \frac{1}{2}(y_{j+\frac{1}{2}} + y_{j-\frac{1}{2}}), \xi_k = \frac{1}{2}(\xi_{k+\frac{1}{2}} + \xi_{k-\frac{1}{2}}), \eta_l = \frac{1}{2}(\eta_{l+\frac{1}{2}} + \eta_{l-\frac{1}{2}})$. The mesh size is denoted by $\Delta x = x_{i+\frac{1}{2}} - x_{i-\frac{1}{2}}, \Delta y = y_{j+\frac{1}{2}} - y_{j-\frac{1}{2}}, \Delta\xi = \xi_{k+\frac{1}{2}} - \xi_{k-\frac{1}{2}}, \Delta\eta = \eta_{l+\frac{1}{2}} - \eta_{l-\frac{1}{2}}$. We define the cell average of f as

$$f_{ijkl} = \frac{1}{\Delta x \Delta y \Delta\xi \Delta\eta}\int_{x_{i-\frac{1}{2}}}^{x_{i+\frac{1}{2}}}\int_{y_{j-\frac{1}{2}}}^{y_{j+\frac{1}{2}}}\int_{\xi_{k-\frac{1}{2}}}^{\xi_{k+\frac{1}{2}}}\int_{\eta_{l-\frac{1}{2}}}^{\eta_{l+\frac{1}{2}}} f(x,y,\xi,\eta,t)d\eta d\xi dy dx.$$

Similar to the 1D case, we approximate $c(x,y)$ by a piecewise bilinear function, and, for convenience, we always provide two interface values of c at each cell interface. When c is smooth at a cell interface, the two potential interface values are identical. We also define the average wave speed in a cell by averaging the four wave speed values at the cell interface:

$$c_{ij} = \frac{1}{4}(c^+_{i-\frac{1}{2},j} + c^-_{i+\frac{1}{2},j} + c^+_{i,j-\frac{1}{2}} + c^-_{i,j+\frac{1}{2}}).$$

The 2D Liouville equation (4.1) can be semidiscretized as

$$(f_{ijkl})_t + \frac{c_{ij}\xi_k}{\Delta x\sqrt{\xi_k^2 + \eta_l^2}}\left(f^-_{i+\frac{1}{2},jkl} - f^+_{i-\frac{1}{2},jkl}\right)$$

$$+ \frac{c_{ij}\eta_l}{\Delta y \sqrt{\xi_k^2 + \eta_l^2}} \left(f^-_{i,j+\frac{1}{2},kl} - f^+_{i,j-\frac{1}{2},kl} \right)$$

$$- \frac{c^-_{i+\frac{1}{2},j} - c^+_{i-\frac{1}{2},j}}{\Delta x \Delta \xi} \sqrt{\xi_k^2 + \eta_l^2} \left(f_{ij,k+\frac{1}{2},l} - f_{ij,k-\frac{1}{2},l} \right)$$

$$- \frac{c^-_{i,j+\frac{1}{2}} - c^+_{i,j-\frac{1}{2}}}{\Delta y \Delta \eta} \sqrt{\xi_k^2 + \eta_l^2} \left(f_{ijk,l+\frac{1}{2}} - f_{ijk,l-\frac{1}{2}} \right)$$

$$= \quad 0,$$

where the interface values $f_{ij,k+\frac{1}{2},l}, f_{ijk,l+\frac{1}{2}}$ are provided by the upwind approximation, and the split interface values $f^-_{i+\frac{1}{2},jkl}, f^+_{i-\frac{1}{2},jkl}, f^-_{i,j+\frac{1}{2},kl}, f^+_{i,j-\frac{1}{2},kl}$ should be obtained using a similar but slightly different algorithm for the 1D case. For example, to evaluate $f^{\pm}_{i+\frac{1}{2},jkl}$ we can extend Algorithm I as

Algorithm I in 2D

- if $\xi_k > 0$

$$f^-_{i+\frac{1}{2},jkl} = f_{ijkl}, \quad \xi_{k_1} = -\xi_k$$

  - if $\left(\frac{C^+_{i+\frac{1}{2},j}}{C^-_{i+\frac{1}{2},j}} \right)^2 (\xi_k)^2 + \left[\left(\frac{C^+_{i+\frac{1}{2},j}}{C^-_{i+\frac{1}{2},j}} \right)^2 - 1 \right] (\eta_l)^2 > 0$

$$\xi^- = \sqrt{ \left(\frac{C^+_{i+\frac{1}{2},j}}{C^-_{i+\frac{1}{2},j}} \right)^2 (\xi_k)^2 + \left[\left(\frac{C^+_{i+\frac{1}{2},j}}{C^-_{i+\frac{1}{2},j}} \right)^2 - 1 \right] (\eta_l)^2 }$$

    - if $\xi_{k'} \leq \xi^- < \xi_{k'+1}$ for some k'

$$\gamma^+ = \frac{\xi_k}{\sqrt{(\xi_k)^2 + (\eta_l)^2}}, \quad \gamma^- = \frac{\xi^-}{\sqrt{(\xi')^2 + (\eta_l)^2}}$$

$$\alpha^R = \left(\frac{c^+_{i+\frac{1}{2}} \gamma^- - c^-_{i+\frac{1}{2}} \gamma^+}{c^+_{i+\frac{1}{2}} \gamma^- + c^-_{i+\frac{1}{2}} \gamma^+} \right)^2, \quad \alpha^T = 1 - \alpha^R$$

$$f^+_{i+\frac{1}{2},jkl} = \alpha^T \left(\frac{\xi_{k'+1} - \xi^-}{\Delta \xi} f_{ij,k',l} + \frac{\xi^- - \xi_{k'}}{\Delta \xi} f_{ij,k'+1,l} \right) + \alpha^R f_{i+1,j,k_1,l}$$

    - end
  - else

$$f^+_{i+\frac{1}{2},jkl} = f_{i+1,j,k_1,l}$$

  - end
- if $\xi_k < 0$

$$f^+_{i+\frac{1}{2},jkl} = f_{i+1,jkl}, \quad \xi_{k_1} = -\xi_k$$

  - if $\left(\frac{C^-_{i+\frac{1}{2},j}}{C^+_{i+\frac{1}{2},j}} \right)^2 (\xi_k)^2 + \left[\left(\frac{C^-_{i+\frac{1}{2},j}}{C^+_{i+\frac{1}{2},j}} \right)^2 - 1 \right] (\eta_l)^2 > 0$

$$\xi^+ = -\sqrt{ \left(\frac{C^-_{i+\frac{1}{2},j}}{C^+_{i+\frac{1}{2},j}} \right)^2 (\xi_k)^2 + \left[\left(\frac{C^-_{i+\frac{1}{2},j}}{C^+_{i+\frac{1}{2},j}} \right)^2 - 1 \right] (\eta_l)^2 }$$

    - if $\xi_{k'} \leq \xi^+ < \xi_{k'+1}$ for some k'

$$\gamma^+ = \frac{|\xi^+|}{\sqrt{(\xi^+)^2 + (\eta_l)^2}}, \quad \gamma^- = \frac{|\xi_k|}{\sqrt{(\xi_k)^2 + (\eta_l)^2}}$$

$$\alpha^R = \left(\frac{c^+_{i+\frac{1}{2}}\gamma^- - c^-_{i+\frac{1}{2}}\gamma^+}{c^+_{i+\frac{1}{2}}\gamma^- + c^-_{i+\frac{1}{2}}\gamma^+} \right)^2, \quad \alpha^T = 1 - \alpha^R$$

$$f^-_{i+\frac{1}{2},jkl} = \alpha^T \left(\frac{\xi_{k'+1} - \xi^+}{\Delta \xi} f_{i+1,j,k',l} + \frac{\xi^+ - \xi_{k'}}{\Delta \xi} f_{i+1,j,k'+1,l} \right)$$
$$+ \alpha^R f_{ij,k_1,l}$$

- end
- else

$$f^-_{i+\frac{1}{2},jkl} = f_{i,j,k_1,l} \text{ where } \xi_{k_1} = -\xi_k$$

- end

The flux $f^\pm_{i,j+\frac{1}{2},kl}$ can be constructed similarly.

As introduced in section 2, the essential difference between the 1D and 2D flux definitions is that in the 2D case, the phenomenon that a wave is completely reflected at the interface does occur, while in 1D, the transmission and reflection waves always coexist at the interface.

Since the wave speed $c \in W^{1,\infty}$, this scheme, similar to the 1D scheme, is also subject to a hyperbolic CFL condition under which the scheme is positive.

5. Numerical examples. In this section we present numerical examples to demonstrate the validity of the proposed scheme and to study the numerical accuracy. In the numerical computations the second order TVD Runge–Kutta time discretization [40] is used. We use the second order scheme with the van Leer slope limiter in constructing the numerical fluxes except for Example 5.2.

Example 5.1. A 1D problem with exact L^∞-solution. Consider the 1D Liouville equation

$$(5.1) \qquad\qquad f_t + c(x)\text{sign}(\xi)f_x - c_x|\xi|f_\xi = 0$$

with a discontinuous wave speed given by

$$c(x) = \begin{cases} 0.6 & x < 0 \\ 0.2 & x > 0. \end{cases}$$

The initial data is given by

$$(5.2) \qquad f(x,\xi,0) = \begin{cases} 1 & x < 0, \xi > 0, \sqrt{x^2 + 4\xi^2} < 1, \\ 1 & x > 0, \xi < 0, \sqrt{x^2 + \xi^2} < 1, \\ 0 & \text{otherwise.} \end{cases}$$

In this example the reflection and transmission coefficients α^R, α^T at the interface are $\alpha^R = \frac{1}{4}, \alpha^T = \frac{3}{4}$. The exact solution for f at $t = 1$ is given by
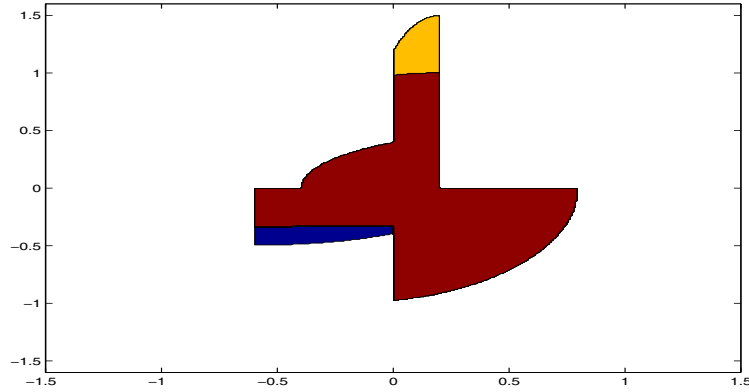
FIG. 5.1. *Example 5.1, the nonzero part of the exact solution $f(x,\xi,1)$ depicted on the 400×400 mesh. The horizontal axis is the position, the vertical axis is the slowness.*

$$f(x,\xi,1) = \begin{cases} \alpha^T & 0 < x < 0.2, \quad \sqrt{1-(0.2-x)^2} < \xi < 1.5\sqrt{1-(3x-0.6)^2}; \\ 1 & 0 < x < 0.2, \quad 0 < \xi < \sqrt{1-(0.2-x)^2}; \\ 1 & 0 < x < 0.8, \quad -\sqrt{1-(x+0.2)^2} < \xi < 0; \\ 1 & -0.4 < x < 0, \quad 0 < \xi < \frac{1}{2}\sqrt{1-(x-0.6)^2}; \\ 1 & -0.6 < x < 0, \quad -\frac{1}{3}\sqrt{1-\left(\frac{x}{3}+0.2\right)^2} < \xi < 0; \\ \alpha^R & -0.6 < x < 0, \quad -\frac{1}{2}\sqrt{1-(x+0.6)^2} < \xi < -\frac{1}{3}\sqrt{1-\left(\frac{x}{3}+0.2\right)^2}; \\ 0 & \text{otherwise}, \end{cases}$$

(5.3)

as shown in Figure 5.1.

We are also interested in computing the moments of f, which include the density

$$\rho(x,t) = \int f(x,\xi,t)d\xi$$

and the averaged slowness

$$u(x,t) = \int f(x,\xi,t)\xi d\xi \bigg/ \rho(x,t).$$

At $t = 1$, the exact density is

$$
\rho(x,1) = \begin{cases}
\sqrt{1 - (x + 0.2)^2} & 0.2 < x < 0.8; \\[2mm]
1.5\alpha^T \sqrt{1 - (3x - 0.6)^2} + \alpha^R \sqrt{1 - (0.2 - x)^2} \\
+\sqrt{1 - (x + 0.2)^2} & 0 < x < 0.2; \\[2mm]
\dfrac{\alpha^T}{3} \sqrt{1 - \left(\dfrac{x}{3} + 0.2\right)^2} + \dfrac{\alpha^R}{2} \sqrt{1 - (x + 0.6)^2} & -0.6 < x < -0.4; \\[2mm]
\dfrac{\alpha^T}{3} \sqrt{1 - \left(\dfrac{x}{3} + 0.2\right)^2} + \dfrac{\alpha^R}{2} \sqrt{1 - (x + 0.6)^2} \\
+\dfrac{1}{2} \sqrt{1 - (x - 0.6)^2} & -0.4 < x < 0, \\[2mm]
0 & \text{otherwise.}
\end{cases}
$$

(5.4)

The averaged slowness only has definition in $[-0.6, 0.8]$ since the density is zero outside this interval. The exact averaged slowness in $[-0.6, 0.8]$ is

$$
u(x,1) = \frac{1}{2\rho(x,1)} \begin{cases}
-\left[1 - (x + 0.2)^2\right] & 0.2 < x < 0.8; \\[2mm]
2.25\alpha^T \left[1 - (3x - 0.6)^2\right] + \alpha^R \left[1 - (0.2 - x)^2\right] \\
-\left[1 - (x + 0.2)^2\right] & 0 < x < 0.2; \\[2mm]
\dfrac{-\alpha^T}{9} \left[1 - \left(\dfrac{x}{3} + 0.2\right)^2\right] - \dfrac{\alpha^R}{4} \left[1 - (x + 0.6)^2\right] & -0.6 < x < -0.4; \\[2mm]
\dfrac{-\alpha^T}{9} \left[1 - \left(\dfrac{x}{3} + 0.2\right)^2\right] - \dfrac{\alpha^R}{4} \left[1 - (x + 0.6)^2\right] \\
+\dfrac{1}{4} \left[1 - (x - 0.6)^2\right] & -0.4 < x < 0.
\end{cases}
$$

(5.5)

We choose the time step as $\Delta t = \frac{1}{2}\Delta\xi$. The computational domain is chosen as $[x, \xi] \in [-1.5, 1.5] \times [-1.6, 1.6]$. Table 5.1 compares the l^1-error of the numerical solutions for f, ρ on $[-1.5, 1.5]$ and u on $[-0.6, 0.8]$ computed with different meshes, respectively.

The convergence rate of f in the l^1-norm is shown to be about 0.74. This agrees with the well-established theory [30, 42], that the l^1-error by finite difference scheme for a discontinuous solution of a linear hyperbolic equation is at most half order. The convergence rate of ρ and u are shown to be about 0.74 and 0.98, respectively, since the solutions also contain discontinuities away from the interface.

Figure 5.2 shows the numerical density ρ and averaged slowness u computed with a 400×400 cell along with the exact solutions in the physical space.

Example 5.2. Computing the physical observables of a 1D problem with measure-valued solution. Consider the 1D Liouville equation (5.1), where the wave speed is a

TABLE 5.1
l^1 error of the numerical solutions with different meshes.

meshes	50×50	100×100	200×200	400×400
f	0.179090	0.104788	0.064989	0.038535
ρ	0.124361	0.079007	0.043248	0.025187
u	0.143083	0.063068	0.043079	0.019870
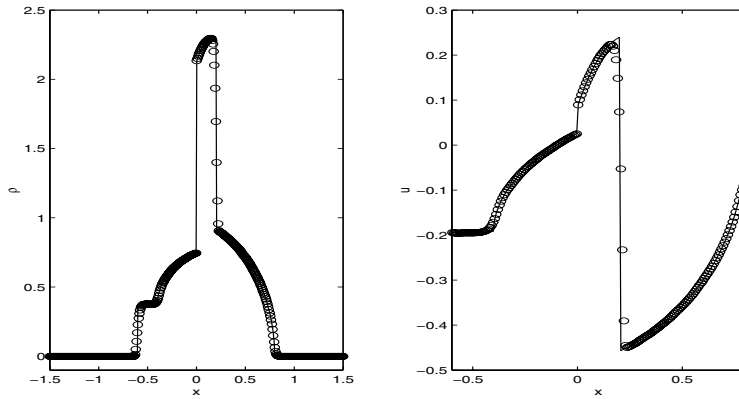
FIG. 5.2. *Example 5.1, the density ρ and averaged slowness u at $t = 1$. Solid line: the exact solution; "o": the numerical solutions using the 400×400 mesh. Left: the density ρ; Right: the averaged slowness u.*

well-shaped function

$$c(x) = \begin{cases} 0.6 & -0.4 < x < 0.4 \\ 1 & \text{else} \end{cases}$$

and the initial data is a delta-function

$$(5.6) \qquad\qquad f(x, \xi, 0) = \delta(\xi - w(x))$$

with

$$(5.7) \qquad w(x) = \begin{cases} 0.5, & x \leq -1.6; \\ 0.5 - \dfrac{0.4}{(1.6)^2}(x + 1.6)^2, & -1.6 < x \leq 0; \\ -0.5 + \dfrac{0.4}{(1.6)^2}(x - 1.6)^2, & 0 < x < 1.6; \\ -0.5, & x \geq 1.6. \end{cases}$$

Figure 5.2 plots $w(x)$ in dashed lines.

In this example we are interested in the approximation of the density

$$\rho(x, t) = \int f(x, \xi, t)d\xi,$$
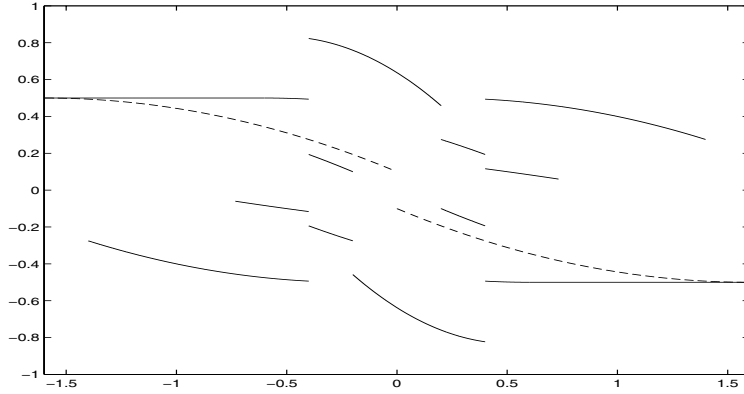
FIG. 5.3. *Example* 5.2, *slowness. Dashed line: the initial slowness* $w(x)$; *Solid line: the slowness at* $t = 1$. *The horizontal axis is the position, the vertical axis is the slowness.*

and the averaged slowness

$$u(x,t) = \frac{\int f(x,\xi,t)\xi d\xi}{\int f(x,\xi,t)d\xi} \, .$$

In the computation, we first approximate the delta function initial data (5.6) by a discrete delta function [16]:

$$(5.8) \qquad \delta_\beta(x) = \begin{cases} \dfrac{1}{\beta}\left(1 - \left|\dfrac{x}{\beta}\right|\right), & \left|\dfrac{x}{\beta}\right| \le 1 \, , \\ 0, & \left|\dfrac{x}{\beta}\right| > 1 \, . \end{cases}$$

If $|\xi_j - w(x_i)| < \beta$, set $f_{ij}^0 = \frac{1}{\beta}\big(1 - |\frac{\xi_j - w(x_i)}{\beta}|\big)$, and $f_{ij}^0 = 0$ otherwise. The choice of the discrete delta function support size β will be made more precise later. We then use the Hamiltonian-preserving scheme to solve the Liouville equation (5.1). Then the moments are recovered by

$$\rho_i^n = \sum_j f_{ij}^n \Delta\xi, \quad u_i^n = \left(\sum_j f_{ij}^n \xi_j \Delta\xi\right) \Big/ \rho_i^n.$$

With partial transmissions and reflections, the exact multivalued slowness at $t = 1$ is depicted as the solid line in Figure 5.3.

In this example the reflection and transmission coefficients α^R, α^T at the wave speed interface are $\alpha^R = \dfrac{1}{16}, \alpha^T = \dfrac{15}{16}$. At $t = 1$, the exact density and averaged

slowness are given by

$$(5.9) \quad \rho(x,1) = \begin{cases} 1, & -1.6 < x < -1.4; \\ 1 + \alpha^R, & -1.4 < x < -0.4 - 1/3; \\ 1 + \alpha^R + 0.6\alpha^T, & -0.4 - 1/3 < x < -0.4; \\ 1 + \alpha^R + \alpha^T/0.6, & -0.4 < x < -0.2; \\ \alpha^T/0.3, & -0.2 < x < 0.2; \\ 1 + \alpha^R + \alpha^T/0.6, & 0.2 < x < 0.4; \\ 1 + \alpha^R + 0.6\alpha^T, & 0.4 < x < 0.4 + 1/3; \\ 1 + \alpha^R, & 0.4 + 1/3 < x < 1.4; \\ 1, & 1.4 < x < 1.6; \end{cases}$$

and

$$u(x,1) = \frac{1}{\rho(x,1)} \begin{cases} 0.5, & -1.6 < x < -1.4; \\ 0.5 - \alpha^R \Upsilon(x + 0.2), & -1.4 < x < -0.4 - \frac{1}{3}; \\ 0.5 - \alpha^R \Upsilon(x + 0.2) - 0.36\alpha^T \Upsilon(0.6x - 1.16), & -0.4 - \frac{1}{3} < x < -0.6; \\ \Upsilon(x + 0.6) - \alpha^R \Upsilon(x + 0.2) - 0.36\alpha^T \Upsilon(0.6x - 1.16), & -0.6 < x < -0.4; \\ \frac{\alpha^T}{0.36} \Upsilon(\frac{x}{0.6} + \frac{13}{15}) - \Upsilon(x - 1) + \alpha^R \Upsilon(x + 1.8), & -0.4 < x < -0.2; \\ \frac{\alpha^T}{0.36} \Upsilon(\frac{x}{0.6} + \frac{13}{15}) - \frac{\alpha^T}{0.36} \Upsilon(\frac{x}{0.6} - \frac{13}{15}), & -0.2 < x < 0.2; \\ -\frac{\alpha^T}{0.36} \Upsilon(\frac{x}{0.6} - \frac{13}{15}) + \Upsilon(x + 1) - \alpha^R \Upsilon(x - 1.8), & 0.2 < x < 0.4; \\ -\Upsilon(x - 0.6) + \alpha^R \Upsilon(x - 0.2) + 0.36\alpha^T \Upsilon(0.6x + 1.16), & 0.4 < x < 0.6; \\ -0.5 + \alpha^R \Upsilon(x - 0.2) + 0.36\alpha^T \Upsilon(0.6x + 1.16), & 0.6 < x < 0.4 + \frac{1}{3}; \\ -0.5 + \alpha^R \Upsilon(x - 0.2), & 0.4 + \frac{1}{3} < x < 1.4; \\ -0.5, & 1.4 < x < 1.6; \end{cases}$$

(5.10)

with $\Upsilon(x) = 0.5 - \frac{0.4}{(1.6)^2} x^2$.

The time step is chosen as $\Delta t = \frac{1}{2}\Delta\xi$. We will give, respectively, the numerical results computed by the first order Hamiltonian-preserving method and the second order method using the van Leer slope limiter. The choice of β in the first and second order methods are different. In the first order method, we use a linear relation between β and the mesh size $\Delta\xi$: $\beta = \Delta\xi$. In the second order method, this choice does not guarantee the numerical convergence, rather, β must decay to zero slower than $\Delta\xi$. Our numerical experiments indicate that $\beta \sim (\Delta\xi)^{\frac{1}{2}}$ will be appropriate.

Table 5.2 presents the l^1-error of ρ and u computed with several different meshes on the domain $[-1.6, 1.6] \times [-1.2, 1.2]$ by using the first order method. It can be observed that the l^1-convergence order of the numerical solutions is about $1/2$ order. Tables 5.3 and 5.4 present the same errors computed by the second order method with two sets of β's. Clearly, the second order methods give more accurate solutions than the first order method. In comparison between the results by the second order methods with different choices of β, one sees that a smaller β gives more accurate

numerical solutions, but might cause mild oscillations, than a larger one. We do not have a rigorous analysis on the relation between β and $\Delta\xi$ to provide the optimal results by a second order method.

TABLE 5.2
l^1 error of the numerical moments with different meshes $\beta = \Delta\xi$, first order method.

meshes	97×80	197×160	397×320	797×640
ρ	3.3051E-1	2.2438E-1	1.6185E-1	1.1425E-1
u	1.1481E-1	8.4303E-2	6.0016E-2	4.2667E-2

TABLE 5.3
l^1 error of the numerical moments with different meshes $\beta = 5\Delta\xi,\ 7\Delta\xi,\ 10\Delta\xi,\ 14\Delta\xi$ for the four meshes, second order method.

meshes	97×80	197×160	397×320	797×640
ρ	1.8969E-1	9.2800E-2	5.5672E-2	3.3926E-2
u	6.1719E-2	3.1710E-2	1.9006E-2	1.1536E-2

Figure 5.4 shows the numerical solutions of ρ and u using the 797×640 mesh by the first order method along with the exact solutions. The numerical solution captures the correct dynamics and discontinuities, but the resolution is poor even on such a fine mesh. In contrast, Figure 5.5 shows the computed densities ρ using the 797×640 mesh by the second order method with different β's. The results have much higher resolution across the discontinuities than the first order method. However, the numerical density by using $\beta = 14\Delta\xi$ exhibits some small oscillations near the discontinuities between, while the use of a larger $\beta = 42\Delta\xi$ creates no oscillations at the expense of a slight accuracy or resolution loss.

These results show that although the second order method can give more accurate solutions than the first order method, there is a support size parameter β that needs to be properly chosen in order to compromise between convergence and accuracy of the numerical solution. It is not clear how to choose β *a priori*. In the future we will study the feasibility of introducing the decomposition technique proposed in [25] into such a problem with measure-valued data, which could avoid such an inconvenience as well as improve the numerical accuracy and resolution.

Example 5.3. Computing the physical observables of a 2D problem with a L^∞ solution. Consider the 2D Liouville equation (4.1) with a discontinuous wave speed

$$c(x, y) = \begin{cases} 2 & y > 0 \\ 1 & y < 0 \end{cases}$$

and a smooth initial data

$$f(x, y, \xi, \eta, 0) = \frac{1}{\pi c_3 c_4}\exp\left(-\left(\frac{x}{c_1}\right)^2 - \left(\frac{y + 0.1}{c_2}\right)^2 - \left(\frac{\xi}{c_3}\right)^2 - \left(\frac{\eta - 0.1}{c_4}\right)^2\right),$$

where $c_1 = 0.03, c_3 = 0.05, c_2 = c_4 = 0.025$.

In this example we aim at computing the density which is the zeroth moment of the density distribution

$$\text{(5.11)} \qquad \rho(x, y, t) = \int\int f(x, y, \xi, \eta, t)d\xi d\eta.$$

l^1 error of the numerical moments with different meshes $\beta = 15\Delta\xi,\ 21\Delta\xi,\ 30\Delta\xi,\ 42\Delta\xi$ for the four meshes, second order method.

meshes	97×80	197×160	397×320	797×640
ρ	4.3791E-1	2.0464E-1	9.0273E-2	3.7545E-2
u	1.3585E-1	6.0953E-2	2.9188E-2	1.2857E-2
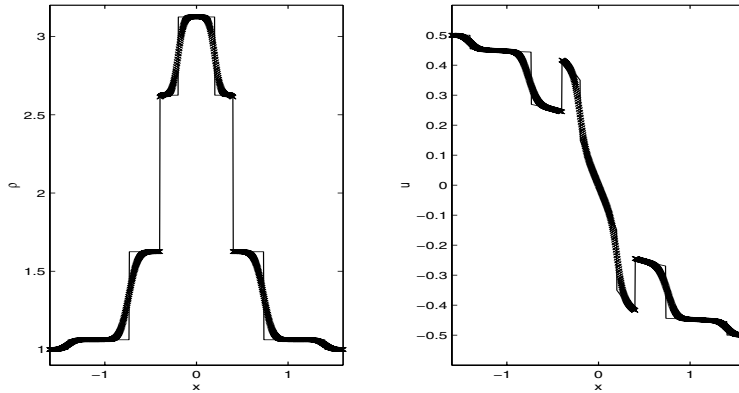
FIG. 5.4. *Example* 5.2, *density* ρ *and averaged slowness* u *at* $t = 1$. *Solid line: the exact solution;* "x": *numerical solutions by first order method using the* 797×640 *mesh. Left:* ρ; *Right:* u.
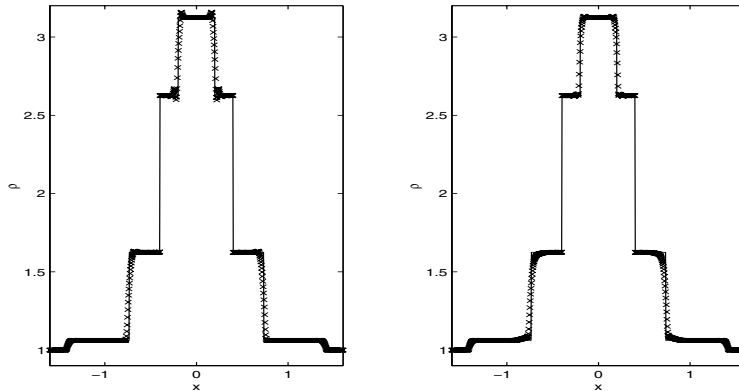
FIG. 5.5. *Example* 5.2, *density* ρ *at* $t = 1$. *Solid line: the exact solution;* "x": *numerical solutions by second order method using the* 797×640 *mesh. Left:* $\beta = 14\Delta\xi$; *Right:* $\beta = 42\Delta\xi$.

The computational domain is chosen to be $[x, y, \xi, \eta] \in [-0.12, 0.12] \times [-0.2, 0.2] \times [-0.2, 0.2] \times [-0.2, 0.2]$.

The reflection and transmission coefficients α^R, α^T at the interface are given by (2.4). The "exact" solution of ρ is obtained by first solving for $f(x, y, \xi, \eta, t)$ analytically, and then evaluating the integral (5.11) on a very fine mesh in the (ξ, η) space.

The time step is chosen as $\Delta t = \frac{1}{3}\Delta x$. Figures 5.6 and 5.8 show, respectively, the numerical density ρ at $t = 0.12, 0.15$ using different meshes along with the exact solution. Figures 5.7 and 5.9 show, respectively, the numerical density ρ on $x = 0$ at
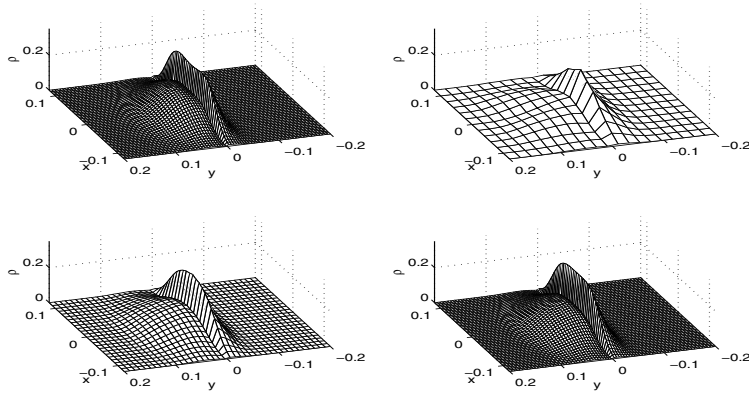
FIG. 5.6. *Example* 5.3, *density* ρ *at* $t = 0.12$. *Upper left: the exact solution; Upper right:* $13 \times 20 \times 14^2$ *mesh; Lower left:* $25 \times 40 \times 26^2$ *mesh; Lower right:* $49 \times 80 \times 50^2$ *mesh.*
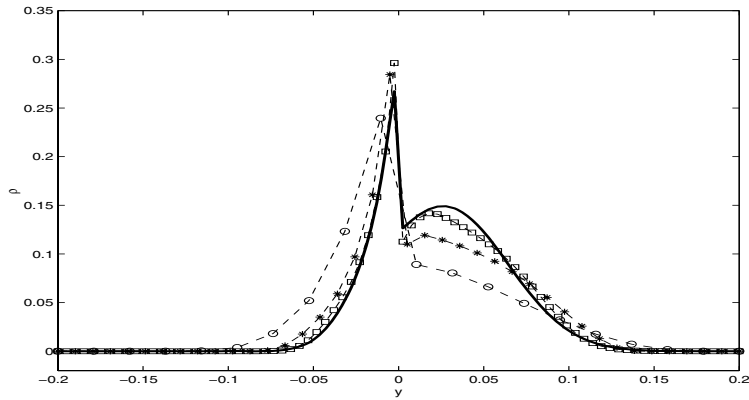
FIG. 5.7. *Example* 5.3, *density* ρ *along* $x = 0$ *at* $t = 0.12$. *Solid line: exact solution; "o":* $13 \times 20 \times 14^2$ *mesh; "*": $25 \times 40 \times 26^2$ *mesh;* "□": $49 \times 80 \times 50^2$ *mesh.*

$t = 0.12, 0.15$ using different meshes along with the exact solution.

Table 5.5 presents the l^1 errors of ρ computed with different meshes in phase space at $t = 0.12, 0.15$. The convergence rate is slightly higher than first order, which does not suffer from the accuracy degeneration of an usual finite difference method for solving the discontinuous solution of a linear hyperbolic equation—which is at most $1/2$ order stated by the well-established theory [30, 42]. This is because the only discontinuity in the solutions is at the interface, which has been taken care of by the Hamiltonian-preserving mechanism, and no linear discontinuity travels to the downstream direction like in the 1D case.

TABLE 5.5
l^1 *error of* ρ *using different meshes.*

meshes	$13 \times 20 \times 14^2$	$25 \times 40 \times 26^2$	$49 \times 80 \times 50^2$
$t = 0.12$	1.241556E-3	5.252852E-4	1.722251E-4
$t = 0.15$	1.244387E-3	6.621391E-4	2.617174E-4
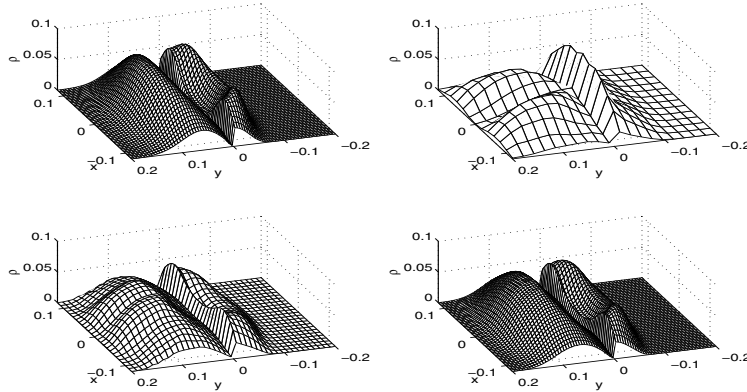
FIG. 5.8. *Example 5.3, density ρ at $t = 0.15$. Upper left: exact solution; Upper right:* $13 \times 20 \times 14^2$ *mesh; Lower left:* $25 \times 40 \times 26^2$ *mesh; Lower right:* $49 \times 80 \times 50^2$ *mesh.*
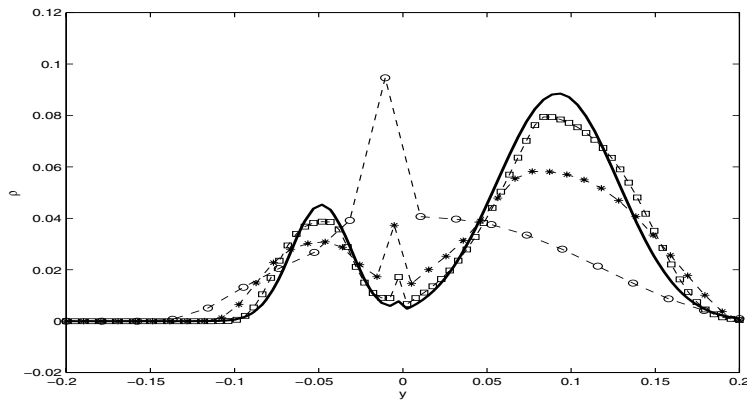
FIG. 5.9. *Example 5.3, density ρ along $x = 0$ at $t = 0.15$. Solid line: exact solution; "o":* $13 \times 20 \times 14^2$ *mesh; "*":* $25 \times 40 \times 26^2$ *mesh; "□":* $49 \times 80 \times 50^2$ *mesh.*

6. Conclusion. In this paper, we extended our previous work [28] to the Liouville equation of geometrical optics with partial transmissions and reflections. Such problems arise in geometrical optics through inhomogeneous media. While still utilizing the constant Hamiltonian structure in constructing the numerical flux, we also account for the transmission and reflection coefficients in the numerical flux. By doing so, the numerical flux automatically absorbs the interface condition. This gives an explicit scheme for the time dependent Liouville equation with discontinuous indices of refraction that can capture correctly the partial transmissions and reflections across the interface. This scheme is subject to a hyperbolic CFL condition, under which the scheme is positive, and stable in both l^1 and l^∞ norms. Numerical experiments are carried out to study the numerical accuracy.

We only extended a finite difference version of the Hamiltonian-preserving scheme developed in [28]. The finite volume version of the method in [28] can also be extended in a similar fashion, but will not be given here.

In the future we will consider analytical issues such as the well-posedness of the problem in a more general context than that discussed in this paper, and the convergence of the numerical scheme. We will also investigate its applications to more

complex interfaces, and develop more effective methods for the measure-valued initial value problem for the same equation.

Acknowledgement. We thank an anonymous referee for his/her valuable comments and suggestions.

REFERENCES

[1] G. Bal, J. B. Keller, G. Papanicolaou, and L. Ryzhik, *Transport theory for acoustic waves with reflection and transmission at interfaces*, Wave Motion, 30 (1999), pp. 303–327.

[2] N. Ben Abdallah, P. Degond, and I. M. Gamba, *Coupling one-dimensional time-dependent classical and quantum transport models*, J. Math. Phys., 43 (2002), pp. 1–24.

[3] J.-D. Benamou, *Big ray tracing: Multivalued travel time field computation using viscosity solutions of the Eikonal equation*, J. Comput. Phys., 128 (1996), pp. 463–474.

[4] J.-D. Benamou, *Direct computation of multivalued phase space solutions for Hamilton-Jacobi equations*, Comm. Pure Appl. Math., 52 (1999), pp. 1443–1475.

[5] J.-D. Benamou, *An introduction to Eulerian geometrical optics* (1992–2002), J. Sci. Comput., 19 (2003), pp. 63–93.

[6] J.-D. Benamou and I. Solliec, *An Eulerian method for capturing caustics*, J. Comput. Phys., 162 (2000), pp. 132–163.

[7] F. Bouchut, *Renormalized solutions to the Vlasov equation with coefficients of bounded variations*, Arch. Ration. Mech. Anal., 157 (2001), pp. 75–90.

[8] F. Bouchut and L. Desvillettes, *On two-dimensional Hamiltonian transport equations with continuous coefficients*, Differential Integral Equations, 14 (2001), pp. 1015–1024.

[9] L.-T. Cheng, M. Kang, S. Osher, H. Shim, and Y.-H. Tsai, *Reflection in a level set framework for geometric optics*, CMES Comput. Model. Eng. Sci., 5 (2004), pp. 347–360.

[10] L.-T. Cheng, H. Liu, and S. Osher, *Computational high-frequency wave propagation using the level set method, with applications to the semi-classical limit of Schrödinger equations*, Commun. Math. Sci., 1 (2003), pp. 593–621.

[11] R. J. DiPerna and P.-L. Lions, *Ordinary differential equations, transport theory, and Sobolev spaces*, Invent. Math., 98 (1989), pp. 511–547.

[12] B. Engquist and O. Runborg, *Multi-phase computations in geometrical optics*, J. Comput. Appl. Math., 74 (1996), pp. 175–192.

[13] B. Engquist and O. Runborg, *Multiphase computations in geometrical optics*, in Hyperbolic Problems: Theory, Numerics, Applications, Internat. Ser. Numer. Math. 129, M. Fey and R. Jeltsch, eds., ETH Zentrum, Zürich, Switzerland, 1998, Birkhauser-Verlag, Basel, 1999.

[14] B. Engquist and O. Runborg, *Computational high frequency wave propagation*, Acta Numer., 12 (2003), pp. 181–266.

[15] B. Engquist, O. Runborg, and A.-K. Tornberg, *High-frequency wave propagation by the segment projection method*, J. Comput. Phys., 178 (2002), pp. 373–390.

[16] B. Engquist, A.-K. Tornberg, and R. Tsai, *Discretization of Dirac delta functions in level set methods*, J. Comput. Phys., 207 (2005), pp. 28–51.

[17] E. Fatemi, B. Engquist, and S. Osher, *Numerical solution of the high frequency asymptotic expansion for the scalar wave equation*, J. Comput. Phys., 120 (1995), pp. 145–155.

[18] S. Fomel and J. A. Sethian, *Fast-phase space computation of multiple arrivals*, Proc. Natl. Acad. Sci., 99 (2002), pp. 7329–7334.

[19] L. Gosse, *Using K-branch entropy solutions for multivalued geometric optics computations*, J. Comput. Phys., 180 (2002), pp. 155–182.

[20] L. Gosse, *Multiphase semiclassical approximation of an electron in a one-dimensional crystalline lattice. II. Impurities, confinement, and Bloch oscillations*, J. Comput. Phys., 201 (2004), pp. 344–375.

[21] L. Gosse, S. Jin, and X. T. Li, *On two moment systems for computing multiphase semiclassical limits of the Schrödinger equation*, Math. Model Methods Appl. Sci., 13 (2003), pp. 1689–1723.

[22] M. Hauray, *On Liouville transport equation with force field in BV_{loc}*, Comm. Partial Differential Equations, 29 (2004), pp. 207–217.

[23] M. Hauray, *On two-dimensional Hamiltonian transport equations with L^p_{loc} coefficients*, Ann. Inst. H. Poincare Anal. Non Linéaire, 20 (2003), pp. 625–644.

[24] S. Jin, H. Liu, S. Osher, and Y.-S.R. Tsai, *Computing multivalued physical observables for the semiclassical limit of the Schrödinger equation*, J. Comput. Phys., 205 (2005), pp. 222–241.

[25] S. Jin, H. Liu, S. Osher, and Y.-S.R. Tsai, *Computing multi-valued physical observables for high frequency limit of symmetric hyperbolic systems*, J. Comput. Phys., 210 (2005), pp. 497–518.

[26] S. Jin and S. Osher, *A level set method for the computation of multivalued solutions to quasilinear hyperbolic PDEs and Hamilton-Jacobi equations*, Commun. Math. Sci., 1 (2003), pp. 575–591.

[27] S. Jin and X. Wen, *Hamiltonian-preserving schemes for the Liouville equation with discontinuous potentials*, Commun. Math. Sci., 3 (2005), pp. 285–315.

[28] S. Jin and X. Wen, *Hamiltonian-preserving schemes for the Liouville equation of geometrical optics with discontinuous local wave speeds*, J. Comput. Phys. 214 (2006), pp. 672–697.

[29] S. Jin and X. Wen, *The l^1-stability of a Hamiltonian-preserving scheme for the Liouville equation with discontinuous potentials*, Math. Comp., submitted.

[30] N. N. Kuznetsov, *On stable methods for solving nonlinear first order partial differential equations in the class of discontinuous functions*, Topics in Numerical Analysis, III, Proc. Roy. Irish Acad. Conf., J. J. H. Miller, ed., Academic Press, London, 1977, pp. 183–197.

[31] R. J. LeVeque, *Numerical Methods for Conservation Laws*, Birkhäuser-Verlag, Basel, 1990.

[32] R. J. LeVeque and C. Zhang, *The immersed interface method for acoustic wave equations with discontinuous coefficients*, Wave Motion, 25 (1997), pp. 237–263.

[33] L. Miller, *Refraction of high-frequency waves density by sharp interfaces and semiclassical measures at the boundary*, J. Math. Pures Appl. (9), 79 (2000), pp. 227–269.

[34] S. Osher, L.-T. Cheng, M. Kang, H. Shim, and Y.-H. Tsai, *Geometric optics in a phase-space-based level set and Eulerian framework*, J. Comput. Phys., 179 (2002), pp. 622–648.

[35] B. Perthame and C.-W. Shu, *On positivity preserving finite volume schemes for Euler equations*, Numer. Math., 73 (1996), pp. 119–130.

[36] B. Perthame and C. Simeoni, *A kinetic scheme for the Saint-Venant system with a source term*, Calcolo, 38 (2001), pp. 201–231.

[37] O. Runborg, *Some new results in multiphase geometrical optics*, M2AN Math. Model. Numer. Anal., 34 (2000), pp. 1203–1231.

[38] L. Ryzhik, G. Papanicolaou, and J. B. Keller, *Transport equations for elastic and other waves in random media*, Wave Motion, 24 (1996), pp. 327–370.

[39] L. Ryzhik, G. Papanicolaou, and J. B. Keller, *Transport equations for waves in a half space*, Comm. Partial Differential Equations, 22 (1997), pp. 1869–1910.

[40] C.-W. Shu and S. Osher, *Efficient implementation of essentially nonoscillatory shock capturing scheme*, J. Comput. Phys., 77 (1988), pp. 439–471.

[41] W. W. Symes and J. Qian, *A slowness matching Eulerian method for multivalued solutions of Eikonal equations*, J. Sci. Comput., 19 (2003), pp. 501–526. Special issue in honor of the sixtieth birthday of Stanley Osher.

[42] T. Tang and Z. H. Teng, *The sharpness of Kuznetsov's $O(\sqrt{\Delta x})$ L^1-error estimate for monotone difference schemes*, Math. Comp., 64 (1995), pp. 581–589.